# Supporting Information

## Smith et al. 10.1073/pnas.1008026107

### SI Materials and Methods

**Chemicals.** Chemicals were analytical grade and obtained from Bioshops, Inc. unless otherwise specified. Urea concentrations were confirmed by refractometry (1).

**Protein Purification.** Myristoylated hisactophilin was purified as described previously (2) with an additional separation by acetonitrile gradient RP-HPLC. Briefly, cells containing myristoylated hisactophilin were resuspended in Tris buffer pH 8 and lysed using an Emulsiflex C-5 emulsifier (Avestin, Inc.). Next, 0.5% (wt/vol) CHAPS was added to the crude cell lysate which was then incubated for 2 h at 4 °C to facilitate solubilization of membrane-bound hisactophilin. Hisactophilin was purified using DEAE (Biorad, Inc.) anion exchange chromatography, followed by gel filtration using a HiLoad 26/60 Superdex 75 column (GE Healthcare). Myristoylated and nonmyristoylated hisactophilin eluted in well-separated peaks in RP-HPLC chromatography using a $C_{18}$ column (Waters, Inc.) and an acetonitrile gradient. The level of myristoylation of hisactophilin was typically ~80%. Purified protein was exchanged into 25 mM ammonium carbonate, lyophilized, and stored at −80 °C. Homogeneity of purified protein was verified by mass spectrometry (3).

**Equilibrium, Folding, and Unfolding Measurements.** Equilibrium denaturation curves were measured as described previously (4). Stock protein solution was prepared by dissolving lyophilized hisactophilin to a concentration of 2 mg·mL$^{-1}$ in either 500 mM MES, 500 mM potassium phosphate, or 500 mM glycine at the appropriate pH. Protein stock was diluted 10-fold in water and stock urea to the desired final concentration of urea. Samples were equilibrated at 25.0 °C in a water bath for at least 10 half-lives as measured for kinetic folding–unfolding transitions. Samples were monitored by fluorescence using a Fluorolog3-22 spectrofluorometer (Horiba-Jobin-Yvon Spex, Inc.) as described previously with excitation and emission wavelengths of 277 and 306 nm, respectively (4, 5). Equilibrium denaturation and renaturation curves were also monitored by circular dichroism at 227 nm using a J715 spectropolarimeter (Jasco, Inc.) as described previously (2). Kinetic folding and unfolding reactions with half-lives greater than ~15 s were measured by manual mixing using the Fluorolog3-22. Faster folding–unfolding rates were measured using the Fluorolog3-22 interfaced with a SFM4/Q (Molecular Kinetics, Inc.). Kinetic data were fit using the Biokine 2.1 software (Molecular Kinetics, Inc.). Data were then fit to a two-state unfolding model (Table S1) using the binomial extrapolation method as described previously (5). Applicability of the two-state model is supported by the agreement of kinetic and equilibrium data (Table S1) and by agreement between fluorescence and circular dichroism results (Table S2). Due to long extrapolations to folding conditions at 0 M urea, the $m$ values of some kinetic data show systematic deviations from equilibrium data. However, $C_{mid}$ values from equilibrium and kinetic experiments are similar, which supports the two-state folding model (6).

**NMR Experiments.** $^{15}$N-labeled hisactophilin was prepared by growing *Escherichia coli* in M9 minimal media with $^{15}NH_4$-Cl (Cambridge Isotopes) as the sole nitrogen source as described previously (7). Resonance assignments were made using 2D homonuclear NOESY and total correlation spectroscopy (TOCSY) as well as 3D $^{15}$N-edited heteronuclear single quantum coherence (HSQC) NOESY and HSQC TOCSY spectra of myristoylated hisactophilin at pH 6.8. Assignments for nonmyristoylated hisactophilin were used as a starting point for making assignments of the myristoylated protein, followed by confirmation and extension using standard procedures (8). Assignments were obtained for the α-proton and amide nitrogen–proton resonances of 96 of 118 residues; the majority of unassigned residues are in the loop consisting of residues 25–32. $^1$H spectra for lineshape analysis were acquired at pH 6.1 at temperatures ranging from 1–25 °C. Lineshapes were simulated using equations from ref. 9.

### SI Results

**Analysis Of Switch Energetics Using Thermodynamic Cycles.** The pH dependence of $\Delta\Delta G_{U\text{-}F}$ can be understood using thermodynamic cycles (Fig. S1) (6). $\Delta\Delta G_{U\text{-}F}$ is the change in the Gibbs free energy of unfolding upon myristoylation:

$$\Delta\Delta G_{U\text{-}F} = \Delta G_{U\text{-}F,\mathrm{myr}} - \Delta G_{U\text{-}F,\mathrm{nonmyr}} \qquad \textbf{[S1]}$$

where the subscripts myr and nonmyr represent myristoylated and nonmyristoylated hisactophilin, respectively. $\Delta\Delta G_{U\text{-}F}$ varies with pH from 3.15 kcal·mol$^{-1}$ at high pH where the myristoyl group is sequestered inside the protein ($myr_{seq}$) to 1.13 kcal·mol$^{-1}$ at lower pH where the myristoyl group is accessible ($myr_{acc}$). The apparent free energy change for switching from the sequestered to the accessible state for the myristoylated protein relative to the nonmyristoylated protein, $\Delta G_{switch}$, can be expressed in terms of the change in $\Delta\Delta G_{U\text{-}F}$ from low to high pH:

$$\Delta G_{\mathrm{switch}} = \Delta\Delta G_{U\text{-}F,\mathrm{high\,pH}} - \Delta\Delta G_{U\text{-}F,\mathrm{low\,pH}} \qquad \textbf{[S2]}$$

Substituting Eq. **S1** into Eq. **S2** gives (Fig. S1)

$$\Delta G_{\mathrm{switch}} = \Delta G_{U\text{-}F,\mathrm{myr,high\,pH}} - \Delta G_{U\text{-}F,\mathrm{nonmyr,high\,pH}} - (\Delta G_{U\text{-}F,\mathrm{myr,low\,pH}} - \Delta G_{U\text{-}F,\mathrm{nonmyr,low\,pH}}) \qquad \textbf{[S3]}$$

We assume that the change in the free energy of the unfolded state with pH is not altered upon myristoylation, i.e., $\Delta G_{U(\mathrm{low}\rightarrow\mathrm{high})\mathrm{myr}} = G_{U\mathrm{high,myr}} - G_{U\mathrm{low,myr}} = \Delta G_{U(\mathrm{low}\rightarrow\mathrm{high})\mathrm{nonmyr}} = G_{U\mathrm{high,nonmyr}} - G_{U\mathrm{low,nonmyr}}$excluding energy contributions for the free amino terminal group in the nonmyristoylated protein, which is not present in the myristoylated protein. In addition, we assume that the contribution of the amino terminal ionizable group does not contribute to protein stability because it is highly exposed to solvent in the folded protein (6, 10). Thus, the amino terminal group makes the same contributions to pH dependence of the energy for folded and unfolded states of nonmyristoylated hisactophilin, and these terms cancel out in the analysis. These are reasonable assumptions because the stability and kinetics are the same for the nonmyristoylated hisactophilin characterized herein and another nonmyristoylated variant hisactophilin containing four additional random coil residues, Gly-Glu-Phe-Gly (GEFG), at the N terminus (4, 10) (Table S1). Using the above assumptions, Eq. **S3** can be simplified as

$$\Delta G_{\mathrm{switch}} = \Delta G_{F,\mathrm{myr(high}\rightarrow\mathrm{low\,pH)}} - \Delta G_{F,\mathrm{nonmuyr(high}\rightarrow\mathrm{low\,pH)}} = \Delta G_{F(\mathrm{nonmyr}\rightarrow\mathrm{myr})\mathrm{low\,pH}} - \Delta G_{F(\mathrm{nonmyr}\rightarrow\mathrm{myr})\mathrm{high\,pH}} \qquad \textbf{[S4]}$$

Thus, $\Delta G_{switch}$ can be interpreted as the coupling energy between the myristoyl group and the sites of protonation involved in

switching from the sequestered to the accessible state with decreasing pH for the myristoylated protein relative to the nonmyristoylated protein (6). Note that the myristoyl group and protonation sites need not interact directly, but may be coupled indirectly through the protein structure (11). The switch energy includes various contributions from inter- and intramolecular interactions, including energy terms due to ionization as well as interactions associated with changes in the myristoyl group environment.

**Fitting the pH dependence of stability changes to a $pK_a$-change model.** Changes in protein stability as a function of pH can be expressed in terms of the Wyman linkage equation:

$$\frac{d}{d\mathrm{pH}}(\Delta G_{U\text{-}F}) = 2.303 \cdot R \cdot T \cdot [Q_U(\mathrm{pH}) - Q_F(\mathrm{pH})] \qquad \textbf{[S5]}$$

where $Q_U(\mathrm{pH})$ and $Q_F(\mathrm{pH})$ represent the number of protons bound at a given pH to the unfolded and folded protein, respectively, and $R$ and $T$ are the universal gas constant and temperature (in kelvin), respectively (12, 13). For hisactophilin, an analogous equation for the pH dependence of $\Delta\Delta G_{U\text{-}F}$ can be written in terms of the number of protons bound to the accessible ($Q_{\mathrm{acc}}(\mathrm{pH})$) and sequestered ($Q_{\mathrm{seq}}(\mathrm{pH})$) states, which may be expressed in terms of the $pK_a$ of residues affected by myristoyl switching, using the nonmyristoylated protein as a reference:

$$\frac{d}{d\mathrm{pH}}(\Delta\Delta G_{U\text{-}F}) = 2.303 \cdot R \cdot T \cdot [Q_{\mathrm{acc}}(\mathrm{pH}) - Q_{\mathrm{seq}}(\mathrm{pH})] + C. \qquad \textbf{[S6]}$$

The constant, $C$, represents the effect of myristoylation on stability at limiting low pH. Integration of Eq. **S6** from a reference pH (pH = 1) chosen outside the range of the myristoyl switch gives

$$\Delta\Delta G_{U\text{-}F}(\mathrm{pH}) = -R \cdot T \cdot n \cdot \ln\left(\frac{(1+10^{\mathrm{pH}-\mathrm{pK}_{\mathrm{a,acc}}}) \cdot (1+10^{1-\mathrm{pK}_{\mathrm{a,seq}}})}{(1+10^{1-\mathrm{pK}_{\mathrm{a,acc}}}) \cdot (1+10^{\mathrm{pH}-\mathrm{pK}_{\mathrm{a,seq}}})}\right) + C \qquad \textbf{[S7]}$$

where $n$ represents the number of ionizable groups whose apparent $pK_a$ values are perturbed upon myristoyl switching and $pK_{a,acc}$ and $pK_{a,seq}$ represent the average apparent $pK_a$ values for these groups in the $myr_{acc}$ and $myr_{seq}$ states, respectively. This derivation assumes that perturbations occur only in folded and not in unfolded hisactophilin. This model is supported by differences in the pH dependence of membrane binding measured for folded myristoylated and nonmyristoylated hisactophilin (14), and the reasonable assumption that there are no residual interactions of the myristoyl group in the unfolded protein that alter $pK_a$ values. Also, comparison of the two nonmyristoylated constructs (the construct used herein of the wild-type sequence, and the construct with additional GEFG, at the N terminus; refs. 4, 10) shows that the N-terminal amino group does not contribute to myristoyl switching (see above). In addition, isoelectric focusing shows that the pI of hisactophilin changes very little (~0.1 pH unit) upon myristoylation or addition of four N-terminal amino acids (Fig. S2*C*). The addition of GEFG to the N-terminus changes the pI in a similar way as the myristoyl group but does not affect the pH dependence of global protein stability. Thus, the measured pH dependence of $\Delta\Delta G_{U\text{-}F}$ is not caused by global changes in pI upon myristoylation but rather arises from changes in $pK_a$ of specific residues accompanying switching from the $myr_{acc}$ to the $myr_{seq}$ state.

Fitting of the pH dependence of $\Delta\Delta G_{U\text{-}F}$ to Eq. **S7** indicates that the total number of protons taken up upon switching is ~1.5 (Fig. S2). However, the exact number of histidines involved in taking up these protons is not well defined by the data. The quality of the fit is slightly better for low values of $n$ based on $\chi^2$ values. The data can alternatively be fit in terms of two histidines with different values of $pK_{a,acc}$ and $pK_{a,seq}$ according to

$$\Delta\Delta G_{U\text{-}F}(\mathrm{pH}) = -R \cdot T \cdot \sum_{n=1}^{2} \ln\left(\frac{(1+10^{\mathrm{pH}-\mathrm{pK}_{\mathrm{a,acc}}(n)}) \cdot (1+10^{1-\mathrm{pK}_{\mathrm{a,seq}}(n)})}{(1+10^{1-\mathrm{pK}_{\mathrm{a,acc}}(n)}) \cdot (1+10^{\mathrm{pH}-\mathrm{pK}_{\mathrm{a,seq}}(n)})}\right) + C \qquad \textbf{[S8]}$$

where $n$ represents the index of the ionizable group. The fits did not converge when all parameters were allowed to vary. However, by fixing values of $pK_{a,acc}$ and $pK_{a,seq}$ for one ionizable group based on apparent $pK_a$ values observed by NMR (e.g., for H91 and H75, see main text, Fig. 4 *D* and *E* and following section), values of $pK_{a,acc}$ and $pK_{a,seq}$ could be fit for the second ionizable group, and the fitted lines accounted well for the observed data; the data were not well fit by a single ionizable group (Fig. S2*B*). These results show that a single ionizable group with $pK_{a,acc}$ and $pK_{a,seq}$ corresponding to apparent $pK_a$ values observed in the NMR data can account for most but not all of the observed pH dependence of $\Delta\Delta G_{U\text{-}F}$. The data can be well fit using just two ionizable groups with $pK_{a,acc}$ and $pK_{a,seq}$ in the range of values observed in the NMR data. Fitting does not exclude that more than two ionizable groups may be involved, but it supports the conclusion that at least one histidine with a $pK_{a,seq}$ value of ~6 (see also Fig. S5) and a higher value of $pK_{a,acc}$ of ~7 likely plays a key role in switching. The identity of the ionizable groups involved in switching was further investigated from the patterns in observed chemical shift changes, described below.

**NMR Data Analyses.** ***Chemical shift changes upon myristoylation.*** There are extensive chemical shift changes upon myristoylation ($\Delta\delta_{\mathrm{myr}}$). The changes are illustrated in the 1D $^1$H spectrum in the changes observed for various down-field amide resonances that are well resolved in the spectrum of nonmyristoylated hisactophilin but not in the spectrum of the myristoylated protein (Fig. S3*A*). Another obvious change is an additional peak in the up-field region of the spectrum for myristoylated hisactophilin (Fig. S3*A*). The chemical shift for I85 $\delta CH_3$ is −0.800 and −0.732 ppm in nonmyristoylated and myristoylated hisactophilin, respectively, and there is a new peak for the latter at −0.824 ppm, corresponding to the terminal $CH_3$ of the myristoyl group (Fig. S3 *B* and *C*). The up-field shift for the myristoyl resonance likely occurs due to the close proximity of the terminal methyl to the aromatic rings of F6 and F113 in the model of myristoylated hisactophilin (Fig. 4 *A* and *B*; see also below). The myristoyl methyl chemical shift was observed to change from pH 7.7 to pH 5.7, where the myristoyl resonance becomes overlapped with other peaks (Fig. S7*B*). This pH dependence most likely reflects a combination of the myristoyl switch and $pK_{a,seq}$ of ~6 (see main text). A single peak was observed for the myristoyl group at all pH values at 25 °C, indicating fast exchange between $myr_{seq}$ and $myr_{acc}$ states. Evidence of line broadening was observed at lower temperatures, where rates were slowed to the intermediate exchange rate regime (see below).

***Model of myristoylated hisactophilin.*** The position of the sequestered myristoyl group in the hisactophilin core was modeled based on the NMR structure of nonmyristoylated protein (PDB ID code 1HCD) because no substantial changes in NOEs were observed in $^{15}$N-edited NOESY-HSQC spectra upon myristoylation. Using the University of California, San Francisco program Chimera, the myristoyl group was modeled into the core of the structure of nonmyristoylated hisactophilin using

the observed NOEs between the myristoyl methyl group and the amide protons of F6, I85, I93, and F113 as distance restraints (15). Subsequently, using the NAMD and VMD software, the structure was energy minimized and then subjected to a brief molecular mechanics simulation using the CHARMM force field to reduce steric clashes (16, 17).

***Identification of ionizable groups that control the myristoyl switch from changes in chemical shift as a function of pH.*** Chemical shifts are sensitive to changes in electrostatic environment caused by pH (8). Thus, amide groups in close proximity to an ionizable group can exhibit pH-dependent changes in chemical shift that reflect the $pK_a$ of that ionizable group. If a given amide group is in rapid exchange on the NMR timescale between states that differ in electrostatic environment (i.e., $myr_{seq}$ and $myr_{acc}$ states, in which ionizable groups have different apparent $pK_a$ values and hence different partial charges), its observed chemical shift will be a population weighted average of its chemical shifts in the different states (18, 19). We focus here on identifying ionizable groups exhibiting $pK_a$ changes that could account for the fits of the pH dependence of the switch energetic (Fig. S2). These may be expected to exhibit $pK_{a,acc}$ of ~7–7.5 and $pK_{a,seq}$ of ~6 in the $myr_{acc}$ and $myr_{seq}$ states, respectively (Figs. S2, S4*F*, and S5). Nonmyristoylated hisactophilin is a model of the $myr_{acc}$ state (see above), in which ionizable groups involved in the switch will exhibit $pK_{a,acc}$. In myristoylated hisactophilin, both $pK_{a,acc}$ and $pK_{a,seq}$ may contribute to the observed pH dependence, with the observed overall behavior depending on the magnitude of the chemical shift changes associated with each $pK_a$. Although the population of certain states may be low, e.g., <5%, they may still be identified by NMR if they undergo relatively large chemical shift changes. Similar to the observation of "invisible" states with low population in NMR relaxation dispersion analyses (20). The magnitudes of the chemical shift changes caused by changes in charge of ionizable groups involved in switching are likely to be larger in general for the $myr_{seq}$ state if the ionizable group is more buried than in $myr_{acc}$ state where it is more exposed to solvent. Thus, the ionization of important histidines around a $pK_{a,seq}$ of ~6 can still be observed even though the pH is ~1 unit below the $pK_{switch}$ because the $myr_{seq}$ state is sufficiently populated and exhibits sufficiently large chemical shift changes to allow for observation by NMR.

An apparent $pK_a$ of ~6 is observed for a large proportion of amides distributed throughout the protein (Fig. S5*A*). It should be noted that this shift in $pK_a$ is not observed for all amides and many amides exhibit no change in apparent $pK_a$; these amides tend to be at the periphery of the protein structure, and farthest from the myristoyl group (Fig. S6*A*). The magnitudes of the chemical shift changes associated with an apparent $pK_a$ of ~6 are largest for amides on one side of the protein structure (Fig. 4*F*) and suggest possible histidine residues that control the switch (see main text). It should be noted that the magnitude and direction of the chemical shift changes is not in general consistent with a shift toward random coil (e.g., H75, H91, or I85; Fig. 4 *D* and *E*, and Fig. S5*B*) and a similar apparent $pK_a$ is observed for the methyl of the myristoyl group and methyl of I85 (Fig. S7 *A* and *B*). A logical interpretation of these results is as follows: In the $myr_{seq}$ state, the myristoyl group is buried in the hydrophobic core (Fig. 4 *A* and *B*) and histidines controlling the switch have relatively low apparent $pK_{a,seq}$ values (e.g., one is at ~6). The low values may result from a hydrophobic environment and/or proximity of positively charged groups. Upon protonation of the buried histidines many amides throughout the protein show chemical shift changes as a consequence of highly cooperative perturbations arising from the generation of buried positively charged groups. The magnitude of the changes in chemical shift caused by changes in charge of ionizable groups involved in switching are likely to be larger in general in $myr_{seq}$ if the ionisable group is more buried than in $myr_{acc}$ where it is more exposed and effects are shielded by the solvent.

***Estimation of exchange rates by NMR lineshape analysis.*** NMR lineshape analysis has been used to study the dynamics of many different groups in proteins that undergo exchange processes such as ring flipping of aromatic residues (21), global protein folding–unfolding rates (22), and *cis-trans*-isomerization (9). The dynamics of the myristoyl switch can be characterized by $k_{out}$, the rate constant for changing from the $myr_{seq}$ to the $myr_{acc}$ state, and $k_{in}$, the rate constant for changing from the $myr_{acc}$ to $myr_{seq}$ state (9, 23). In order to estimate the values of these rate constants, we analyzed exchange effects manifested in the lineshape of the myristoyl methyl group by measuring 1D $^1$H spectra as a function of temperature (Fig. S7*C*). These analyses reveal that at 25 °C the myristoyl group exhibits minimal line broadening, indicating that the exchange between $myr_{seq}$ and $myr_{acc}$ is fast on the NMR timescale. In contrast, at 1 °C pronounced line broadening is observed, indicating that exchange has slowed, becoming intermediate on the NMR timescale. From simulation of the lineshapes, at 1 °C, $k_{in}$ and $k_{out}$ are estimated as ~400 and ~3,600 $s^{-1}$, respectively. At 25 °C, due to less line broadening, the simulated lineshapes are less sensitive to the values of $k_{in}$ and $k_{out}$, for which lower limits are estimated as ~55,000 and ~120,000 $s^{-1}$, respectively. The simulations give a reasonable estimate of the exchange rates, although the uncertainties in the rates are significant (Fig. S7*D*). The values of $k_{in}$ and $k_{out}$ at 25 °C correspond to a 69% $myr_{seq}$ and 31% $myr_{acc}$, which is similar to the expected populations of $myr_{seq}$ and $myr_{acc}$ determined from the equilibrium $\Delta\Delta G_{U\text{-}F}$ values (Fig. 1*B*).


1. Pace CN (1986) Determination and analysis of urea and guanidine hydrochloride denaturation curves. *Methods Enzymol* 131:266–280.
2. Liu C, et al. (2001) Thermodynamics of denaturation of hisactophilin, a beta-trefoil protein. *Biochemistry* 40:3817–327.
3. Scheel J, et al. (1989) Hisactophilin, a histidine-rich actin-binding protein from Dictyostelium discoideum. *J Biol Chem* 264:2832–289.
4. Wong HJ, Stathopulos PB, Bonner JM, Sawyer M, Meiering EM (2004) Non-linear effects of temperature and urea on the thermodynamics and kinetics of folding and unfolding of hisactophilin. *J Mol Biol* 344:1089–1107.
5. Liu C, Gaspar JA, Wong HJ, Meiering EM (2002) Conserved and nonconserved features of the folding pathway of hisactophilin, a beta-trefoil protein. *Protein Sci* 11:669–679.
6. Fersht A (1999) *Structure and Mechanism in Protein Science: A Guide to Enzyme Catalysis and Protein Folding* (Freeman, New York), 508–614.
7. Houliston RS, Liu C, Singh LM, Meiering EM (2002) pH and urea dependence of amide hydrogen-deuterium exchange rates in the beta-trefoil protein hisactophilin. *Biochemistry* 41:1182–1194.
8. Wuthrich K (1986) *NMR of Proteins and Nucleic Acids* (Wiley, New York), 1–44.
9. Duggan BM, Craik DJ (1997) Conformational dynamics of thyroid hormones by variable temperature nuclear magnetic resonance: The role of side chain rotations and cisoid/transoid interconversions. *J Med Chem* 40:2259–2265.
10. Habazettl J, et al. (1992) Structure of hisactophilin is similar to interleukin-1 beta and fibroblast growth factor. *Nature* 359:855–858.
11. Horovitz A, Fersht AR (1990) Strategy for analysing the co-operativity of intramolecular interactions in peptides and proteins. *J Mol Biol* 214:613–617.
12. Cho JH, Sato S, Raleigh DP (2004) Thermodynamics and kinetics of non-native interactions in protein folding: a single point mutant significantly stabilizes the N-terminal domain of L9 by modulating non-native interactions in the denatured state. *J Mol Biol* 338:827–837.
13. Tanford C (1968) Protein denaturation. *Adv Protein Chem* 23:121–282.
14. Hanakam F, Gerisch G, Lotz S, Alt T, Seelig A (1996) Binding of hisactophilin I and II to lipid membranes is controlled by a pH-dependent myristoyl-histidine switch. *Biochemistry* 35:11036–11044.
15. Pettersen EF, et al. (2004) UCSF Chimera—a visualization system for exploratory research and analysis. *J Comput Chem* 25:1605–1612.
16. Humphrey W, Dalke A, Schulten K (1996) VMD: Visual molecular dynamics. *J Mol Graph* 14:33–38.
17. Phillips JC, et al. (2005) Scalable molecular dynamics with NAMD. *J Comput Chem* 26:1781–1802.
18. Cavanagh J (2007) *Protein NMR Spectroscopy : Principles and Practice* (Amsterdam, Academic Press), pp 391–491.
19. Korzhnev DM, et al. (2004) Low-populated folding intermediates of Fyn SH3 characterized by relaxation dispersion NMR. *Nature* 430:586–590.
20. Neudecker P, Lundstrom P, Kay LE (2009) Relaxation dispersion NMR spectroscopy as a tool for detailed studies of protein folding. *Biophys J* 96:2045–2054.

21. Wagner G, Wuthrich K (1978) Dynamic model of globular protein conformations based on NMR studies in solution. *Nature* 275:247–248.
22. Wang M, et al. (2003) Dynamic NMR line-shape analysis demonstrates that the villin headpiece subdomain folds on the microsecond time scale. *J Am Chem Soc* 125:6032–6033.
23. Huang G, Oas TG (1995) Submillisecond folding of monomeric lambda repressor. *Proc Natl Acad Sci USA* 92:6878–6882.

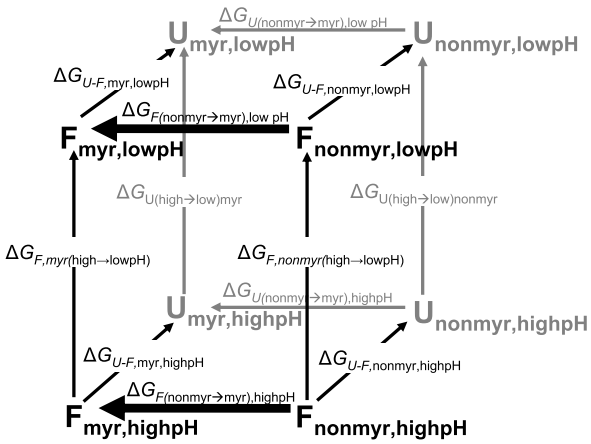


**Fig. S1.** Thermodynamic cycles for measuring $\Delta G_{switch}$. Arrows define the direction from initial to final states. Each arrow is associated with a change in Gibbs free energy ($\Delta G$) that is defined with a subscript. *U* and *F* refer to the unfolded and folded protein, respectively, subscripts lowpH and highpH represent terms corresponding to $myr_{acc}$ and $myr_{seq}$ states, respectively, and subscripts myr and nonmyr represent the myristoylated and nonmyristoylated forms of hisactophilin, respectively. The derivation for $\Delta G_{switch}$ is analogous to the coupling energy derivation described by Fersht (6). $\Delta G_{switch}$ is defined as $\Delta G_{switch} = \Delta G_{F(nonmyr\rightarrow myr)low\ pH} - \Delta G_{F(nonmyr\rightarrow myr)highpH} = \Delta G_{F,myr(high\rightarrow lowpH)} - \Delta G_{F,nonmyr(high\rightarrow lowpH)} = \Delta G_{U\text{-}F,myr,lowpH} - \Delta G_{U\text{-}F,nonmyr,lowpH} - (\Delta G_{U\text{-}F,myr,highpH} - \Delta G_{U\text{-}F,nonmyr,highpH})]$, assuming $\Delta G_{U(high\rightarrow low)myr} = \Delta G_{U(high\rightarrow low)nonmyr}$, i.e., myristoylation has no effect on the pH dependence of the free energy of the unfolded state and so these terms cancel out. Bold arrows illustrate $\Delta G_{F(nonmyr\rightarrow myr)lowpH}$ and $\Delta G_{F(nonmyr\rightarrow myr)highpH}$.

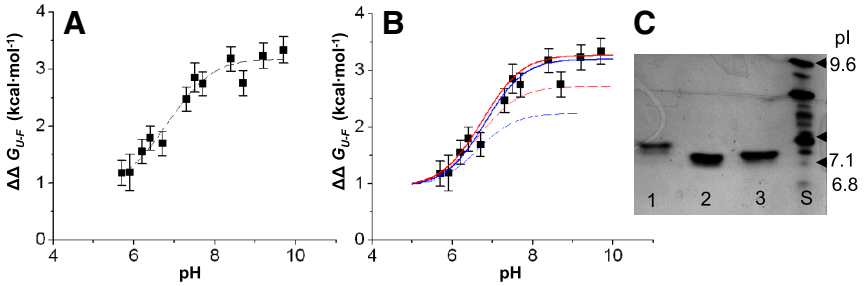


| *n* | 1 | 2 | 5 | 15 | 31 |
|---|---|---|---|---|---|
| $pK_{a,acc}$ | 7.66 | 7.31 | 7.10 | 7.00 | 6.98 |
| $pK_{a,seq}$ | 6.04 | 6.55 | 6.80 | 6.90 | 6.93 |
| $\Delta pK_{a(seq-acc)}$ | -1.62 | -0.74 | -0.30 | -0.10 | -0.05 |
| C (kcal·mol$^{-1}$) | 0.96 | 1.09 | 1.13 | 1.13 | 1.13 |
| $\chi^2$ | 0.034 | 0.035 | 0.036 | 0.036 | 0.036 |
| $H^+$ uptake/release | 1.62 | 1.51 | 1.49 | 1.47 | 1.45 |

**Fig. S2.** Change in stability upon myristoylation as a function of pH fit to $pK_a$-change model. (*A*) In the graph, the dashed line represents the fit of the data to Eq. **S7**, allowing all parameters (*n*, $pK_{a,acc}$, $pK_{a,seq}$) to vary. The fit converged to a best-fit *n* value of 0.98 ± 0.68 (error estimate is from the fitting program, Origin 5.0). Integration of the curve gives the total number of protons involved in the switch, ~1.5. The data were also fit by fixing *n* to various values, with the values for the remaining fitted parameters summarized in the table. For these, the fitted lines for different values of *n* are extremely similar visually. As *n* increases, the differences in $pK_a$ of the ionizable groups, $\Delta pK_{a(seq-acc)}$, decreases and the $\chi^2$ increases slightly, suggesting that a small number of ionizable groups controls the switch. (*B*) Based on analysis of the pH dependence of chemical shift changes (Fig. 4 *D*–*F*), data were also simulated assuming only two independent ionizable groups controlling the switch using Eq. **S8**. Values of $pK_{a,acc}$ and $pK_{a,seq}$ for one group were fixed to 6.1 and 7.1 (corresponding to the data for H91 in Fig. 4*E*) and the corresponding values for the second ionizable group were allowed to vary. This simulation gave fitted values for the second $pK_{a,acc}$ and $pK_{a,seq}$ of 7.4 and 6.7, respectively (solid red line). When values for $pK_{a,acc}$ and $pK_{a,seq}$ were fixed to 6.0 and 7.3 (based on data for H75 in Fig. 4*D*), this choice gave values of $pK_{a,acc}$ and $pK_{a,seq}$ for the second ionizable group of 7.2 and 6.8, respectively (solid blue line). Dashed lines show data simulations assuming a single ionizable group with $pK_{a,acc}$ and $pK_{a,seq}$ corresponding to the values for H91 (blue) or H75 (red). (*C*) Isoelectric focusing gel electrophoresis of hisactophilin variants. Lanes: 1, nonmyristoylated wild-type hisactophilin; 2, myristoylated myristoylated hisactophilin; 3, nonmyristoylated hisactophilin with additional N-terminal Gly-Glu-Phe-Gly residues. Lane S contains protein markers with pI values labeled. Weak bands at slightly lower pI values for hisactophilin samples correspond to hisactophilin dimers, likely formed by oxidation of Cys 49 during electrophoresis. Dimerization does not affect the stability of hisactophilin (2).

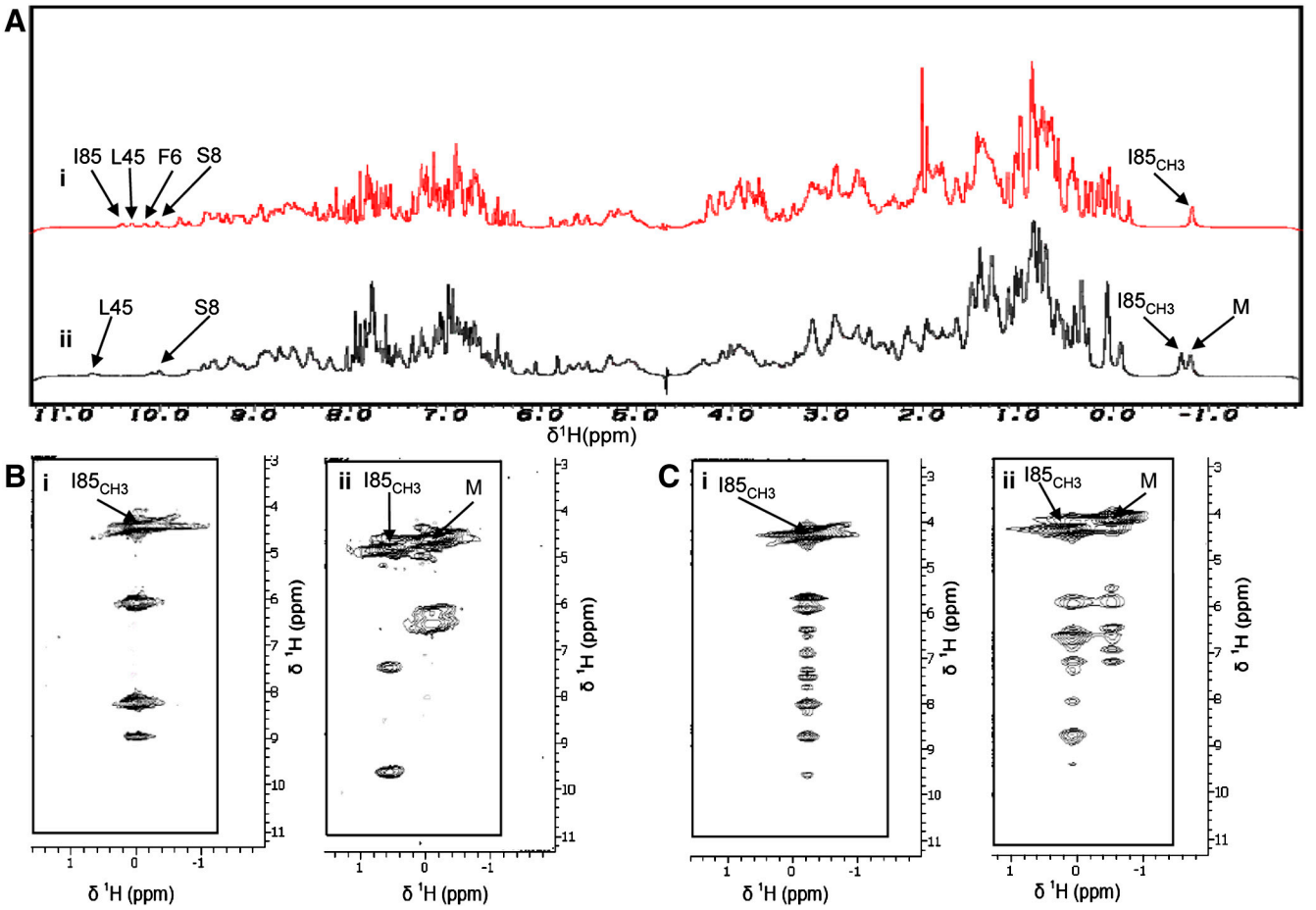


**Fig. S3.** NMR spectral changes upon myristoylation. Spectra in *A–C* show corresponding regions for nonmyristoylated (*i*) and myristoylated (*ii*) hisactophilin. M indicates the resonance for the terminal methyl of the myristoyl group and $I85_{CH3}$ indicates the resonance for the $\delta CH_3$ of I85. (*A*) 1D $^1$H spectra. Various residues exhibiting significant changes (F6, S8, L45, I85) are labeled. (*B*) 2D $^1$H-$^1$H TOCSY and (*C*) 2D $^1$H-$^1$H NOESY strips, showing new peaks observed for the terminal methyl of the myristoyl.

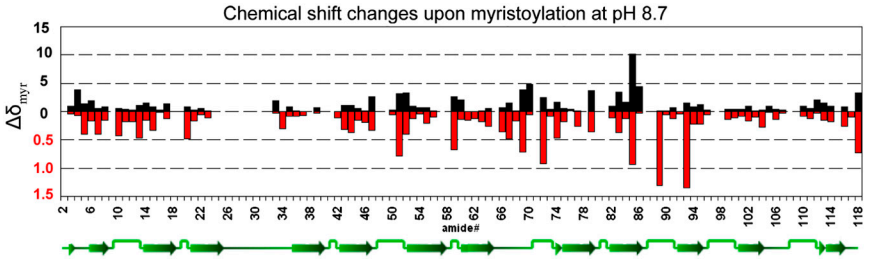


**Fig. S4.** Absolute value of changes in chemical shift, Δδ, upon myristoylation for $^1$H (red) and $^{15}$N (black) of backbone amide groups versus residue number at pH 8.7. The protein secondary structure is shown below the graphs as a green ribbon with β-strands shown as arrows.

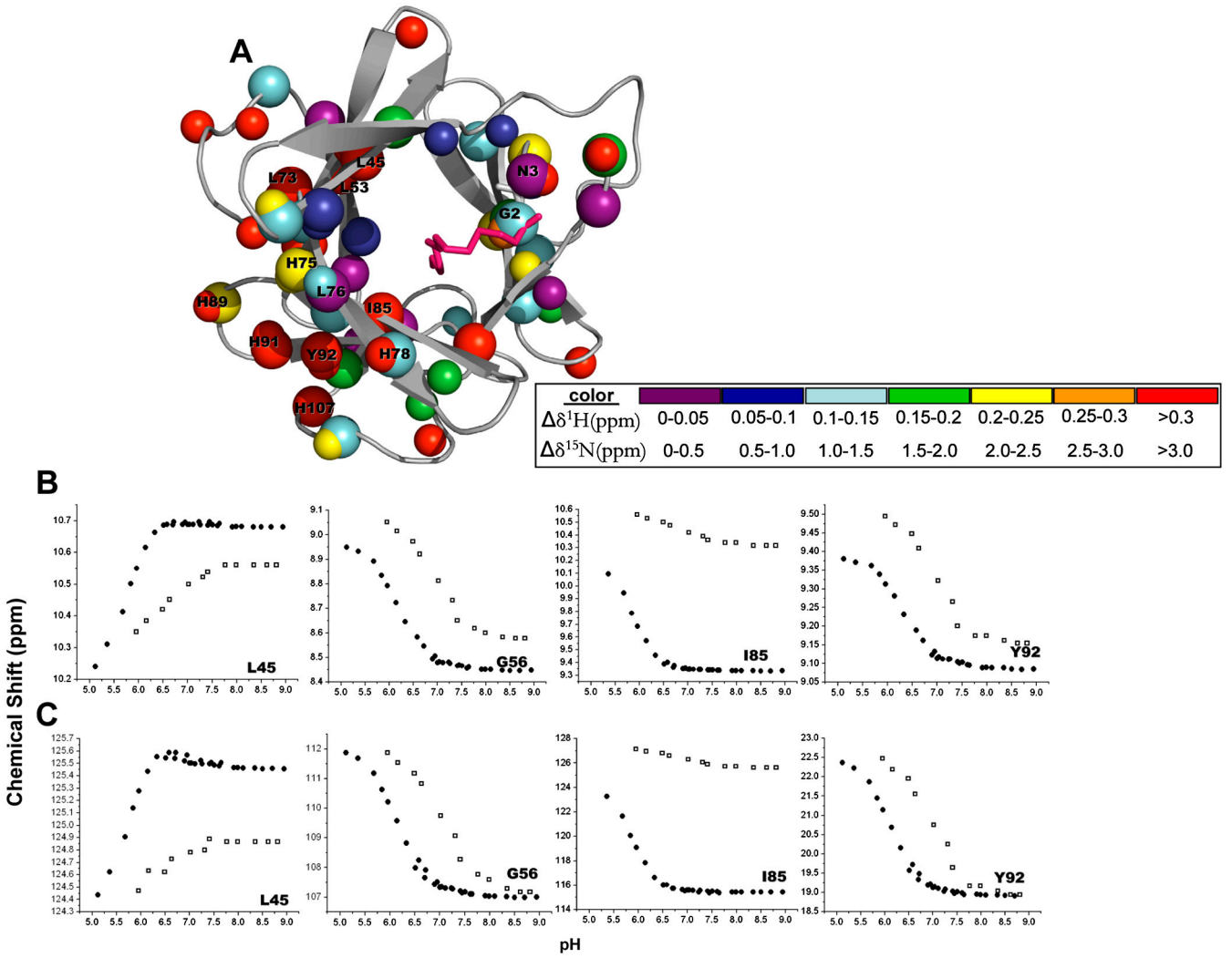


**Fig. S5.** NH resonances monitored by $^{1}H$-$^{15}N$ HSQC that exhibit an apparent $pK_{app}$ value of ~6 in myristoylated hisactophilin. (*A*) Ribbon diagram of myristoylated hisactophilin showing all $^{15}N$ and $^{1}H$ resonances that have a $pK_{app}$ ~6 as spheres, with the myristoyl group (pink) shown in the $myr_{seq}$ conformation. Backbone $^{1}H$ resonances (small spheres) are colored in a rainbow gradient according to their absolute Δδ values upon myristoylation as follows: 0–0.05, purple; 0.05–0.1, blue; 0.1–0.15, cyan; 0.15–0.2, green; 0.2–0.25, yellow; 0.25–0.3, orange; >0.3, red. Backbone $^{15}N$ resonances (large spheres) are colored in a rainbow gradient according to absolute Δδ values as 0–0.5, purple; 0.5–1.0, blue; 1.0–1.5, cyan; 1.5–2.0, green; 2.0–2.5, yellow; 2.5–3.0, orange; >3.0, red. (*B*) Representative plots of δ vs. pH for backbone $^{1}H$ resonances for myristoylated (filled circle) and nonmyristoylated (open square) hisactophilin that show a decrease in $pK_{app}$ from ~7 to ~6 upon myristoylation as also seen for H75 and H91 (Fig. 4 *D* and *E*, main text). Panels are labeled with single residue code and amino acid number. The backbone amide $^{1}H$ resonances exhibiting $pK_{app}$ ~6 in myristoylated hisactophilin include G2, K7, H12, F34, V36, K42, V43, G49, L53, S54, G56, L67, H68, H71, F74, H75, H78, I85, H89, H91, Y92, H107, D110, and I118. (*C*) Representative plots of δ vs. pH plots for backbone $^{15}N$ resonances for myristoylated (●) and nonmyristoylated (□) hisactophilin that show a decrease in $pK_{app}$ from ~7 to ~6 upon myristoylation as also seen for H75 and H91 (Fig. 4 *D* and *E*, main text). Panels are labeled with single residue code and amino acid number. The backbone amide $^{15}N$ resonances showing a $pK_{app}$ ~6 include G2, N3, R4, A5, F6, S8, H9, F13, L14, A16, K42, V43, L45, K46, L53, Q60, V61, S64, H66, L73, F74, H75, L76, H78, I85, K86, H89, S94, and I117. The large number of nuclei exhibiting an apparent $pK_a$ of ~6 in myristoylated hisactophilin indicate that protonation of this ionizable group in the $myr_{seq}$ conformation has effects that are felt throughout the structure, likely due to the ionizable group being in a buried hydrophobic environment and/or near positively charged groups (which also decreases its apparent $pK_a$ value).

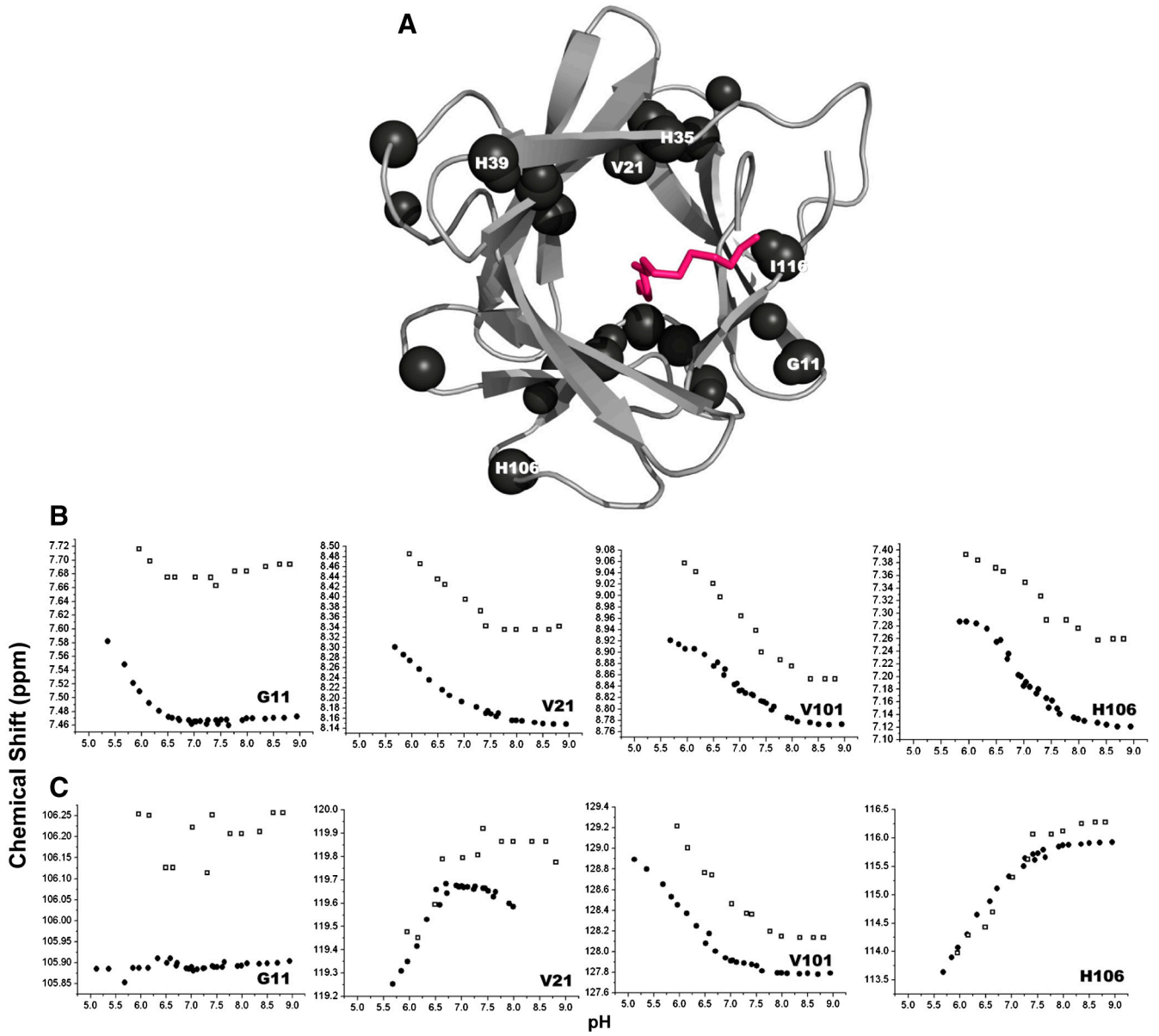


**Fig. S6.** NH resonances monitored by $^{1}H$-$^{15}N$ HSQC that exhibit no significant changes in apparent $pK_{app}$ values upon myristoylation. (*A*) Ribbon diagram of myristoylated hisactophilin illustrating all $^{15}N$ (large black spheres) and $^{1}H$ (small black spheres) that show no significant change in $pK_{app}$ values. The myristoyl (pink) is shown in the $myr_{seq}$ conformation. (*B*) Representative plots of δ vs. pH plots for backbone $^{1}H$ resonances that show no significant changes in $pK_{app}$ upon myristoylation (panels are labeled with single residue code and amino acid number). The amide $^{1}H$ resonances that show no change include G11, E17, A20, V21, H33, H35, H39, A44, G99, V101, S102, K104, H106, E115, and I116. (*C*) Representative plots of δ vs. pH plots for backbone $^{15}N$ resonances that show no significant changes in $pK_{app}$ upon myristoylation (panels are labeled with single residue code and amino acid number). The amide $^{15}N$ resonances that show no change include G11, A20, V21, H35, H39, A44, Y62, H68, H90, S94, G99, H100, V101, T103, H106, and I116. The nuclei that show no change are generally at the periphery of the structure.

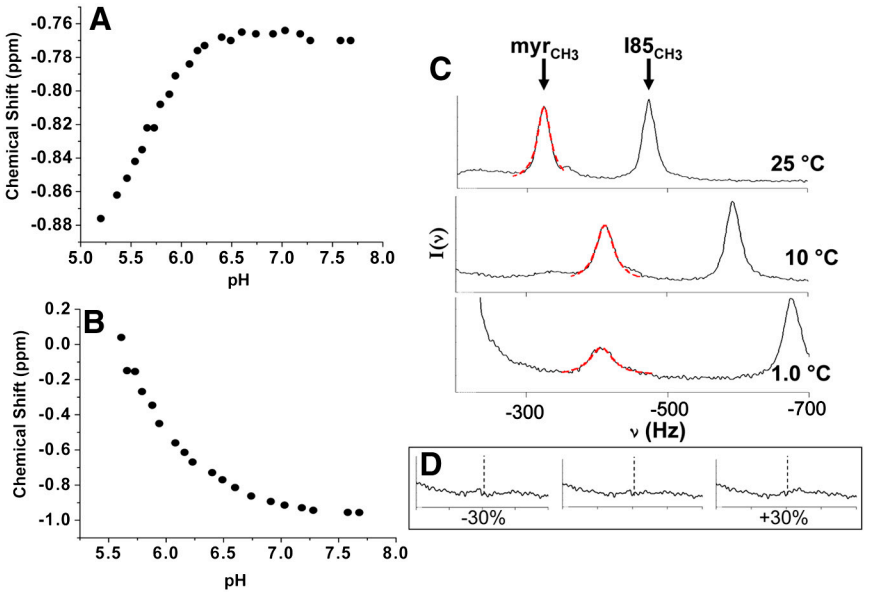


**Fig. S7.** $^1$H NMR lineshape analysis of I85 and myristoyl methyl groups in hisactophilin. One-dimensional $^1$H NMR-monitored pH titration for (*A*) $I85_{\delta CH3}$ and (*B*) myristoyl terminal $CH_3$ groups. Measured chemical shift values, δ, at different pH values are shown by ●. (*C*) Lineshape analysis of dynamics of the myristoyl methyl group as a function of temperature at pH 6.1. Measured NMR spectra are shown as continuous black lines and simulated spectra for the myristoyl terminal $-CH_3$ group are shown as red lines. Lineshapes were simulated as described previously (9). Limiting values of ν and linewidth for $myr_{seq}$ and $myr_{acc}$ in the simulation were estimated from spectra obtained at pH 7.7 and 5.8, respectively. The values of $k_{in}$ and $k_{out}$ used for the simulated peaks at 1, 10, and 25 °C are 400 and 3,600 $s^{-1}$, 7,850 and 25,000 $s^{-1}$, and 55,000 and 120,000 $s^{-1}$, respectively. (*D*) Plots of residuals (i.e., experimental—simulated lineshape data) for different values of $k_{in}$ and $k_{out}$ at 1 °C. Center plot shows residual for reported values of $k_{in}$ and $k_{out}$, left plot shows residual when $k_{in}$ and $k_{out}$ are both set 30% lower than reported values, and right plot shows residual when $k_{in}$ and $k_{out}$ are both set 30% higher than reported values. The residuals give an estimate of effects of changes in the rate constants on the simulated spectra.

**Table S1. Table of fluorescence monitored equilibrium and kinetic parameters for pH 5.7–9.7**

| | | Myristoylated hisactophilin* | | | | | | | Nonmyristoylated hisactophilin* | | | | | | |
|---|---|---|---|---|---|---|---|---|---|---|---|---|---|---|---|
| pH | Kinetic/Equilibrium | $C_{mid}$ | $m_1$[†] | $\Delta G_{U\text{-}F}$[‡] | $k_u$ | $k_f$ | $m_u$[§] | $m_f$[§] | $C_{mid}$ | $m_1$[†] | $\Delta G_{U\text{-}F}$[‡] | $k_u$ | $k_f$ | $m_u$[§] | $m_f$[§] |
| | | M | kcal·mol$^{-1}$·M$^{-1}$ | kcal·mol$^{-1}$ | s$^{-1}$ × 10$^{-5}$ | s$^{-1}$ × 10$^{3}$ | s$^{-1}$·M$^{-1}$ | s$^{-1}$·M$^{-1}$ | M | kcal·mol$^{-1}$·M$^{-1}$ | kcal·mol$^{-1}$ | s$^{-1}$ × 10$^{-5}$ | s$^{-1}$ | s$^{-1}$·M$^{-1}$ | s$^{-1}$·M$^{-1}$ |
| 5.7 | Equilibrium | 1.44 ± 0.07[¶] | 2.34 ± 0.22 | 3.22 ± 0.38 | —— | —— | —— | —— | 0.91 ± 0.03 | 2.63 ± 0.29 | 2.34 ± 0.29 | —— | —— | —— | —— |
| 5.9 | Equilibrium | 2.05 ± 0.23 | 2.40 ± 0.17 | 4.85 ± 0.42 | —— | —— | —— | —— | 1.49 ± 0.06 | 2.20 ± 0.24 | 3.09 ± 0.83 | —— | —— | —— | —— |
| 6.2 | Equilibrium | 2.62 ± 0.41 | 2.43 ± 0.13 | 6.62 ± 0.41 | —— | —— | —— | —— | 2.27 ± 0.03 | 2.64 ± 0.05 | 5.67 ± 0.76 | —— | —— | —— | —— |
| 6.4 | Equilibrium | 3.69 ± 0.03 | 2.09 ± 0.11 | 6.78 ± 0.42 | —— | —— | —— | —— | 2.85 ± 0.02 | 2.32 ± 0.12 | 6.03 ± 0.36 | —— | —— | —— | —— |
| 6.7 | Equilibrium | 3.71 ± 0.02 | 2.19 ± 0.11 | 7.19 ± 0.43 | —— | —— | —— | —— | 2.89 ± 0.03 | 2.43 ± 0.21 | 6.39 ± 0.67 | —— | —— | —— | —— |
| 6.7 | Kinetics | 3.90 ± 0.22 | 1.91 ± 0.007 | 6.75 ± 0.22 | 201 ± 9 | 0.180 ± 0.06 | 0.607 ± 0.01 | −1.30 ± 0.001 | 2.93 ± 0.30 | 1.91 ± 0.071 | 5.59 ± 0.29 | 16.0 ± 4.00 | 2.03 ± 0.797 | .607 ± 0.019 | -1.30 ± 0.07 |
| 7.3 | Equilibrium | 5.11 ± 0.02 | 2.31 ± 0.16 | 9.92 ± 0.82 | —— | —— | —— | —— | 3.93 ± 0.02 | 2.31 ± 0.11 | 7.98 ± 0.45 | —— | —— | —— | —— |
| 7.5 | Equilibrium | 5.30 ± 0.06 | 2.06 ± 0.16 | 8.93 ± 0.96 | —— | —— | —— | —— | 3.96 ± 0.13 | 3.32 ± 0.39 | 7.88 ± 1.52 | —— | —— | —— | —— |
| 7.6 | Equilibrium | 5.53 ± 0.04 | 1.97 ± 0.08 | 8.76 ± 0.40 | —— | —— | —— | —— | 3.86 ± 0.06 | 1.83 ± 0.03 | 8.40 ± 0.92 | —— | —— | —— | —— |
| 7.7 | Equilibrium | 5.68 ± 0.03 | 2.30 ± 0.12 | 11.34 ± 0.67 | —— | —— | —— | —— | 4.38 ± 0.02 | 2.18 ± 0.11 | 8.16 ± 0.32 | —— | —— | —— | —— |
| 7.7 | Kinetics | 5.65 ± 0.13 | 1.87 ± 0.063 | 9.53 ± 1.1 | 13.0 ± 4 | 1.27 ± 0.098 | 0.684 ± 0.054 | -1.18 ± 0.015 | 4.68 ± 0.15 | 1.87 ± 0.027 | 8.25 ± 0.15 | 2.00 ± 0.380 | 22.5 ± 2.13 | .684 ± 0.011 | -1.18 ± 0.01 |
| 8.4 | Equilibrium | 6.14 ± 0.03 | 2.22 ± 0.18 | 10.96 ± 1.07 | —— | —— | —— | —— | 4.64 ± 0.02 | 2.13 ± 0.11 | 8.37 ± 0.53 | —— | —— | —— | —— |
| 8.7 | Equilibrium | 6.72 ± 0.02 | 2.47 ± 0.21 | 13.44 ± 1.38 | —— | —— | —— | —— | 5.38 ± 0.07 | 2.20 ± 0.27 | 9.45 ± 1.24 | —— | —— | —— | —— |
| 8.7 | Kinetics | 6.83 ± 0.17 | 1.96 ± 0.032 | 11.65 ± 0.3 | 0.200 ± 0.091 | 6.99 ± 0.466 | 0.820 ± 0.027 | -1.13 ± 0.012 | 5.59 ± 0.17 | 1.95 ± 0.029 | 10.44 ± 0.16 | 0.254 ± 0.100 | 116 ±190.4 | 0.820 ± 0.01 | -1.13 ± 0.02 |
| 9.2 | Equilibrium | 6.57 ± 0.04 | 2.43 ± 0.34 | 12.93 ± 2.25 | —— | —— | —— | —— | 5.04 ± 0.06 | 2.39 ± 0.55 | 10.21 ± 2.75 | —— | —— | —— | —— |
| 9.7 | Equilibrium | 6.44 ± 0.06 | 2.12 ± 0.19 | 11.52 ± 1.18 | —— | —— | —— | —— | 4.77 ± 0.07 | 2.17 ± 0.35 | 8.99 ± 1.77 | —— | —— | —— | —— |

*Protein concentrations were all ~0.2 mg/mL.

[†]Equilibrium values were fit using a binomial extrapolation with $m_2 = 0.072$.

[‡]$\Delta G_{U\text{-}F}$ were calculated as described in *Materials and Methods*.

[§]Kinetic data were also fit using the binomial extrapolation with $m_{2ref} = 0$ and $m_{2unf} = 0.028$.

[¶]Errors reported are SD.

**Table S2. Comparison of CD and fluorescence data**

| pH | $Cmid_{CD}$, M | $Cmid_{F1}$, M | $m_{1CD}$,* kcal·mol$^{-1}$·M$^{-1}$ | $m_{1FI}$,* kcal·mol$^{-1}$·M$^{-1}$ | $\Delta G_{U\text{-}F,CD}$,† kcal·mol$^{-1}$ | $\Delta G_{U\text{-}F,FI}$,† kcal·mol$^{-1}$ |
|---|---|---|---|---|---|---|
| 5.7 | 1.53 ± 0.03‡ | 1.44 ± 0.07 | 2.63 ± 0.19 | 2.34 ± 0.22 | 3.86 ± 0.35 | 3.22 ± 0.38 |
| 5.9 | 2.07 ± 0.05 | 2.05 ± 0.23 | 2.42 ± 0.15 | 2.40 ± 0.17 | 4.88 ± 0.32 | 4.85 ± 0.42 |
| 6.7 | 3.66 ± 0.02 | 3.71 ± 0.02 | 2.69 ± 0.19 | 2.19 ± 0.11 | 8.30 ± 0.83 | 7.19 ± 0.43 |
| 7.7 | 5.66 ± 0.03 | 5.68 ± 0.03 | 2.23 ± 0.11 | 2.30 ± 0.12 | 10.35 ± 0.58 | 11.34 ± 0.67 |
| 9.2 | 6.64 ± 0.04 | 6.57 ± 1.04 | 2.28 ± 0.23 | 2.43 ± 0.34 | 13.01 ± 3.73 | 12.93 ± 2.25 |

*Equilibrium values were fit using a binomial extrapolation with $m_2 = 0.072$.
†$\Delta G_{U\text{-}F}$ were calculated as described in *Materials and Methods*.
‡Errors reported are SD.